Nano Energy 78 (2020) 105389

Contents lists available at ScienceDirect

Nano Energy

journal homepage: http://www.elsevier.com/locate/nanoen

Stretchable, self-healing, conductive hydrogel fibers for strain sensing and triboelectric energy-harvesting smart textiles

Luyizheng Shuai [a,1], Zi Hao Guo [b,c,1], Panpan Zhang [b], Junmin Wan [a,**], Xiong Pu [b,c,d,*], Zhong Lin Wang [b,c,e,***]

[a] National Engineering Lab of Textile Fiber Materials & Processing Technology, Zhejiang Sci-Tech University, Hangzhou, 310018, China
[b] CAS Center for Excellence in Nanoscience, Beijing Key Laboratory of Micro-Nano Energy and Sensor, Beijing Institute of Nanoenergy and Nanosystems, Chinese Academy of Sciences, Beijing, 100083, China
[c] School of Nanoscience and Technology, University of Chinese Academy of Sciences, Beijing, 100049, China
[d] Center on Nanoenergy Research, School of Chemistry and Chemical Engineering, School of Physical Science and Technology, Guangxi University, Nanning, 530004, China
[e] School of Materials Science and Engineering, Georgia Institute of Technology, Atlanta, GA, 30332-0245, USA

ARTICLE INFO

Keywords:
Hydrogel fiber
Triboelectric nanogenerator
Strain sensor
Stretchable
Self-healing
Smart textile

ABSTRACT

Stretchable conductive fibers are essential for smart electronic textiles (E-textiles). Here, we develop a continuous dry-wet spinning approach to fabricate stretchable, conductive and self-healing hydrogel fibers. By tuning the contents of acrylamide (AAm) and N-acryloylglycinamide (NAGA), the physically cross-linked poly (NAGA-*co*-AAm) (PNA) hydrogel precursor exhibits thermally reversible sol-gel transition, which ensures the success of the spinning process. The obtained PNA hydrogel fiber achieves excellent tensile strength (2.27 Mpa), stretchability (900%), high conductivity (0.69 S m^{-1}), and self-healing capability. With an elastomeric poly (methyl acrylate) (PMA) coating, the PNA/PMA core-sheath fiber shows excellent resistance to water evaporation and absorption. The strain sensing capability of the PNA/PMA fiber is demonstrated for monitoring human body motions. Furthermore, a triboelectric nanogenerator (TENG) textile woven from the PNA/PMA fibers is fabricated to convert mechanical motion energy into electric power. Our stretchable conductive hydrogel fibers suggest great potentials for next-generation multifunctional smart textiles and wearable electronics.

1. Introduction

Smart electronic textiles have been widely investigated along with the booming of wearable electronics by integrating with different electronic devices, which endow the textile various capabilities far beyond conventional warm/fashion functions, such as sensing, actuating, communicating, self-healing, energy generation and storage [1–5]. Stretchable conductive fibers are of vital importance for the development of smart E-textiles. Existing conductive fibers are mainly electronic conductors, which generally have limited stretchability. Wet- or dry-spun carbon nanotube (CNT) fibers, reduced graphene oxide (rGO) fibers, carbon fibers, and metal-coated fibers/yarns are typically not stretchable [6–8]; CNT-, conductive polymer-, or Ag nanowire-filled polymer composite fibers can have certain stretchability, but high conductivity and stretchability can hardly be simultaneously achieved [9–11]; liquid metal-infiltrated tubular fibers are reported but their application is limited due to the use of liquid materials [12]. In contrast, solid polymer-based ionic conductors have been demonstrated to be promising alternatives for stretchable electronics, especially the hydrogels which possibly allow simultaneously the high stretchability, excellent conductivity and multi-functionalities [13,14]. Currently, hydrogels with different polymer networks have been widely developed

* Corresponding author. CAS Center for Excellence in Nanoscience, Beijing Key Laboratory of Micro-Nano Energy and Sensor, Beijing Institute of Nanoenergy and Nanosystems, Chinese Academy of Sciences, Beijing, 100083, China.
** Corresponding author.
*** Corresponding author. CAS Center for Excellence in Nanoscience, Beijing Key Laboratory of Micro-Nano Energy and Sensor, Beijing Institute of Nanoenergy and Nanosystems, Chinese Academy of Sciences, Beijing, 100083, China.
E-mail addresses: wwjm2001@126.com (J. Wan), puxiong@binn.cas.cn (X. Pu), zhong.wang@mse.gatech.edu (Z.L. Wang).
[1] These authors contributed equally.

https://doi.org/10.1016/j.nanoen.2020.105389
Received 16 August 2020; Received in revised form 7 September 2020; Accepted 12 September 2020
Available online 16 September 2020

for applications as electrodes in strain/pressure sensors [15], artificial muscles [16], electroluminescent devices [17], triboelectric nanogenerators (TENG) [18,19], and as electrolytes in batteries/supercapacitors [20]. However, these hydrogels are mainly 2-D films or 3-D monoliths, and the studies on 1-D hydrogel fibers are still limited.

Several strategies have been attempted to fabricate hydrogel fibers. One of the mostly studied approaches is the drawing method. Supramolecular hydrogel fibers cross-linked by functionalized silica colloidal particles had been drawn to mimic spider fibers, obtaining high strength and high damping efficiency, but their conductivity was not mentioned [21,22]. An anti-freezing conductive polyelectrolyte (sodium polyacrylate) hydrogel fiber was drawn, but it was soluble in water at room temperature without protective coatings [23]. Electrospinning had also been tried to realize fibrous hydrogel, but it can only produce nonwoven webs [24]. 1-D hydrogel cables or fibers had been prepared by a mold casting method [25–27]. With microfluidic template as the mold, the size and shape of hydrogel fibers can be better controlled [28,29]. However, this approach is difficult to continuously produce uniform hydrogel fiber at a large scale. Despite the fact that the spinning is the mostly utilized strategy to prepare polymer fibers, it is hardly employed to produce hydrogel fibers. This is mainly due to the poor spinnability of hydrogels and their precursor solutions. Only a few hydrogel fibers were prepared by wet-spinning [30,31] or dynamic-crosslinking-spinning [32], but their mechanical or electrical properties were not fully studied. Therefore, it is still a challenge to continuously fabricate stretchable conductive hydrogel fibers, especially for the electronic-textile-targeted applications.

In this work, a continuous spinning approach is developed for the synthesis of conductive, stretchable and self-healing hydrogel fibers. The reversible gel-to-sol conversion of a physically cross-linked hydrogel precursor, copolymerized with acrylamide (AAm) and N-acryloylglycinamide (NAGA), is achieved at about 80 °C by tuning the content ratio of NAGA and AAm, which allows the success of the dry-wet spinning of poly (NAGA-*co*-AAm) (PNA) hydrogel fibers. The PNA

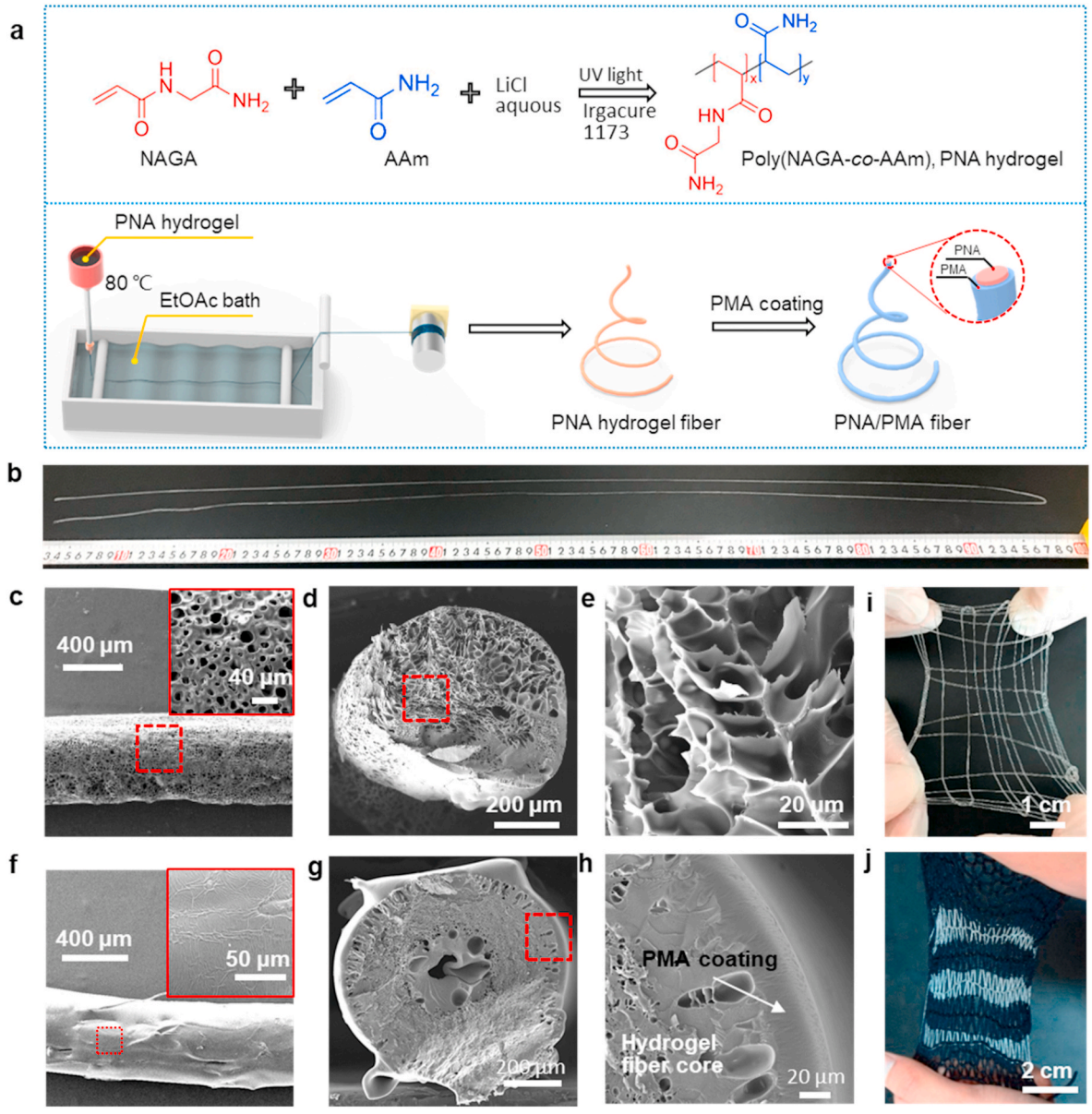

Fig. 1. Preparation of hydrogel and core-sheath fibers. (a) Schematic illustration of the preparation procedures of the PNA hydrogel precursor, PNA hydrogel fibers and PNA/PMA core-sheath fibers. (c) A photo of a 2 m long PNA fiber. (c–e) Scanning electron microscopy (SEM) images a PNA hydrogel fiber. (e) is a magnified view of the rectangular area in d). (f–h) SEM images of a PNA/PMA fiber. (h) is a magnified view of the rectangular area in (g). (i) A web woven from PNA/PMA fibers at stretched state. (j) A fabric knitted from PNA/PMA fibers and wool threads at stretched state.

hydrogel fiber shows high tensile strength (2.27 Mpa), excellent stretchability (900%), good conductivity (0.69 S m^{-1}), and self-healing capability. By further coating the PNA hydrogel fiber with elastomeric poly (methyl acrylate) (PMA), the PNA/PMA core-sheath fiber showed excellent resistance to water evaporation and absorbing. Finally, the PNA/PMA fiber is demonstrated for applications as strain-sensing and triboelectric energy-harvesting E-textiles.

2. Results and discussion

2.1. Fabrication of hydrogel fibers

The spinning fabrication of the hydrogel fibers is schematically illustrated in Fig. 1a. First, the PNA hydrogel was prepared by photo-initiated co-polymerization of NAGA and AAm monomers in 5 wt% LiCl aqueous solution. The weight percentage of NAGA and AAm in aqueous solution is 15 wt% and 5 wt%, respectively. A customer-made spinning setup was used for the continuous spinning of the hydrogel fibers. The PNA hydrogel precursor was transferred into a storage tank, which was heated to about 80 °C so that the hydrogel rapidly softened and changed from a gel state to a viscous sol state. The softened PNA hydrogel was extruded out from the spinning head, and then solidified again into gel fiber in an ethyl acetate coagulation bath at room temperature. After collecting and drying the hydrogel fibers in air, a PMA thin layer was coated on the surface of the hydrogel fibers by a dip-coating method. PMA was obtained using the free radical polymerization method (see SI details), and a 5 wt% PMA solution in ethyl acetate was utilized. The PMA coating was applied to reduce the water evaporation and alleviate the effect of air humidity.

This spinning process has following advantages. First, it is facile for scaled-up and continuous spinning of hydrogel fibers. Fig. 1b shows a 2 m long PNA hydrogel fiber. Second, the water content is well maintained in the final fiber. A hydrogel fiber was prepared without LiCl in the precursor to illustrate this advantage. The water content in the freshly collected hydrogel fibers was measured to be about 67–70 wt%, slightly lower than 80 wt% in the precursor. The porous morphology of the freeze-drying hydrogel fibers also suggested that water molecules were well confined in the polymer networks of the final fibers (Fig. 1c–e). Unlike reported drawn hydrogel fibers with a dried shell [22], the spun hydrogel fibers had porous surface (Fig. 1c) and uniform cross-sectional morphologies (Fig. 1d), suggesting that water was evenly maintained in the fibers. The high water content in the hydrogel fiber ensures its good conductivity. The conductivities of hydrogel fibers were only slightly smaller than their counterpart films (Fig. S1), and the hydrogel fiber with 5 wt% LiCl has a conductivity of 0.69 S m^{-1}. Though higher salt concentration can lead to the higher conductivity, it also increases the viscosity of the hydrogel precursor and thus the difficulty in the extrusion. As for following tested hydrogel fibers, 5 wt% LiCl was always added unless being specifically mentioned. Third, the diameter of the hydrogel fibers can be easily controlled by changing the inner diameter of the spinning head. Fig. S2 showed four hydrogel fibers with different diameters. The diameters of the fibers were about 5–20% larger than that of the inner diameter of the spinning head. Other than mentioned specifically, the diameter of all tested fibers hereafter was about 560 μm.

After dip-coating the hydrogel fiber with the PMA layer, its porous surface turned into a smooth morphology (Fig. 1f). The core-sheath structure can be further confirmed by the cross-sectional images. A thin layer of the PMA coating (~35 μm) is clearly observed to fully wrap the core hydrogel fiber (Fig. 1g–h). The core-sheath fibers can proceed for weaving or knitting fabrics, exhibiting good potentials in E-textiles thanks to their high conductivity and stretchability. The core-sheath fibers were woven into a stretchable web (Fig. 1i), and knitted together with black wool threads into a piece of stretchable fabric (Fig. 1j).

2.2. The mechanism of the spinning process

The thermal-induced reversible transition between solid gel and viscous sol of PNA hydrogel precursor is the key for the success of spinning fabrication of hydrogel fibers. The hydrogel is physically cross-linked by hydrogen bonding among amide groups in the side chains. As illustrated in Fig. 2a, dual hydrogen bonds can be formed among the NAGA segments; while mono-hydrogen bond is formed among AAm segments. It has been reported that the dual hydrogen bonds among bisamides are quite stable and can form strong physical cross-linking; while the hydrogen bonding among single amides is much weaker [33]. This was demonstrated by the fact that the poly (N-acryloylglycinamide) (PNAGA, 20 wt% NAGA) maintained the gel state even increasing the temperature to 80 °C, but the polyacrylamide (PAAm, 20 wt% AAm) was in the sol state at room temperature, as indicated by the inverted vial method (Fig. S3). Therefore, we expect that the sol-gel transition behavior of the PNA hydrogel can be possibly tuned by the content of NAGA and AAm. The optimal gel precursor should be able to change to viscous sol at an appropriate elevated temperature and undergo reversible gelation when cooling down to room temperature, as schemed in Fig. 2b. Three copolymer hydrogel samples were prepared with different NAGA-to-AAm monomer weight ratio, and the total monomer weight percentage was fixed to be 20 wt%. When the NAGA-to-AAm weight ratio is 17/3 (PNA-17/3), no sol transition was observed in the temperature range of 25 °C–80 °C, but gel-to-sol transition occurred at 80 °C and 60 °C for PNA-15/5 PNA-13/7, respectively (Fig. 2c). These results clearly suggests that increasing the AAm content can weaken the physical cross-linking and lower the sol-gel transition temperature by reducing the density of dual hydrogen bonds. This was also demonstrated by the water swelling test at room temperature. PNA-15/5 and PNA-17/3 hydrogel still maintained to be solid form after saturated water swelling, unlike the PAAm and PNA-13/7 hydrogel which can dissolve in the water (Fig. S4).

The thermal-induced gel-to-sol transition of PNA hydrogel can also be explained by the Raman spectroscopy (Fig. 2d). Two peaks belonging to amide I band were observed at 1552 cm^{-1} and 1647 cm^{-1}. The first was assigned to the hydrogen bonding between water molecule and N–H groups in the side chains; while the latter was originated from the hydrogen bonding among NH and C═O groups in the polymer chains [34–36]. In comparison, PNAGA hydrogel has only one main peak at about 1647 cm^{-1}, indicating that the strong dual hydrogen bonding among bisamides can screen the effect of water molecule; while the PAAm hydrogel shows both two peaks, and the peak intensity at 1552 cm^{-1} is high, suggesting the large portion of the hydration of the mono-amide groups (Fig. S5). For PNA-15/5, the intensity of the peak from the NH···O═C hydrogen bonds is much higher than that from water-polymer hydrogen bonds at room temperature, but its intensity decreases significantly at 80 °C due to the largely weakened physical cross-linking at high temperature (Fig. 2d).

The dynamic mechanical analyses of the three PNA hydrogel precursors were examined by a rheometer over a temperature range of 25–90 °C. It is noted that all the samples were tested at swelled states because of the step to remove residual small molecular impurities with DI water. Fig. 2e shows the variation of storage modulus (G') and loss moduli (G'') of PNA-15/5 with the temperature. The G' keeps about one order of magnitude higher than G'' in the temperature range 25–50 °C, correspondent to the gel state; while the G' drops rapidly around 60 °C, and the G' is close to G'' when temperature is higher than 60 °C, confirming the transition to viscous sol due to the softened physical cross-linking. The much larger G' than G'' obtained at room temperature from angular frequency-dependent oscillatory rheology test confirmed the stability of the PNA-15/5 hydrogel at different frequencies (Fig. 2f). In contrast, PNA-17/3 shows no transition to sol state at elevated temperature; while the PNA-13/7 remains to be viscous liquid in the tested temperature range (Fig. S6).

Based on these analyses, it is demonstrated that PNA-15/5 is optimal

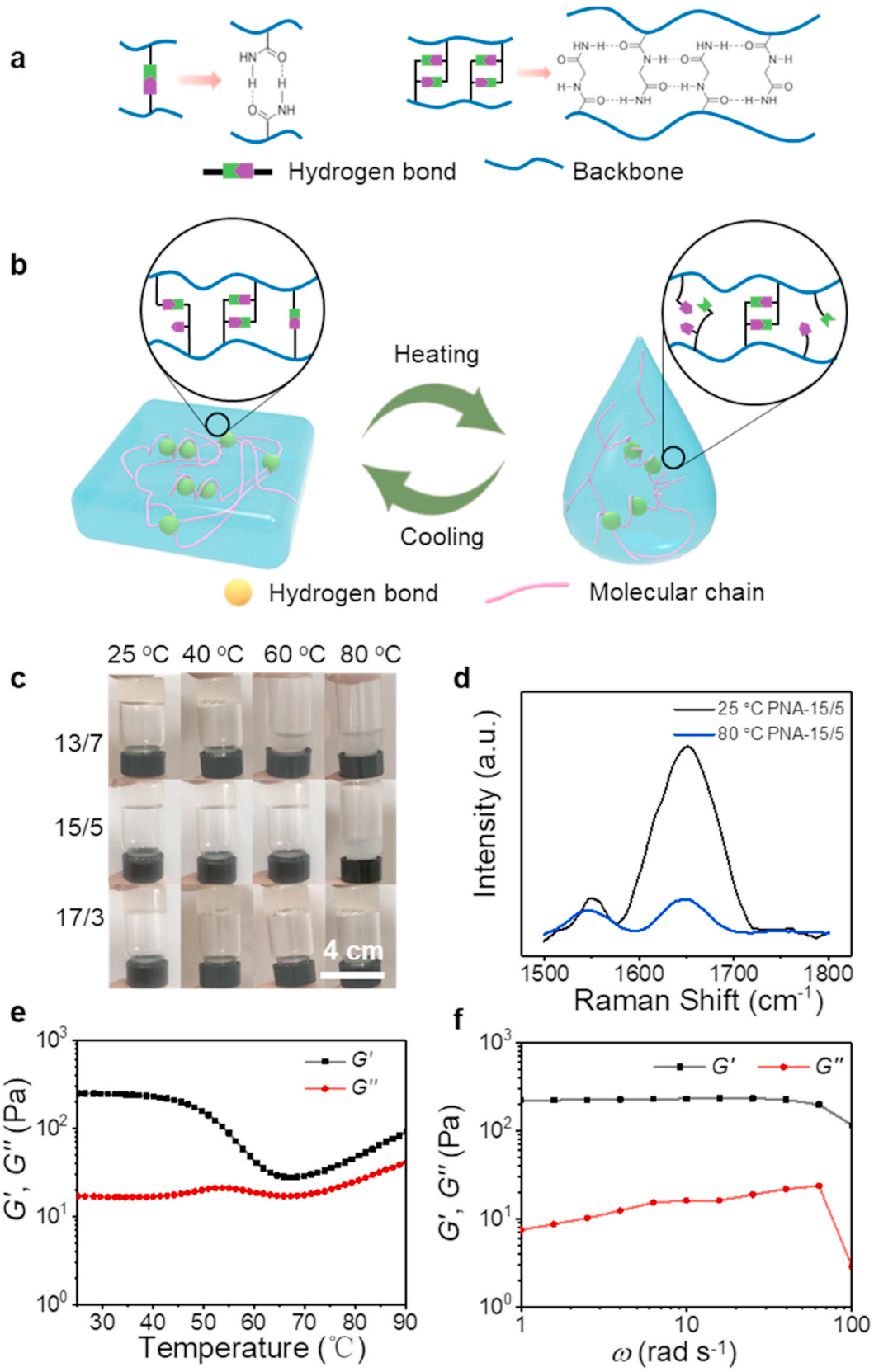

Fig. 2. Mechanism of the thermal sol-gel transition of the PNA hydrogel. (a) scheme of the mono-hydrogen bonding between AAm segments and dual hydrogen bonding between NAGA segments. (b) Scheme of the reversible sol-gel transition of PNA. (c) Photos of inverted vials showing the effect of NAGA-to-AAm weight ratio on the sol-gel transition behavior of the PNA hydrogel. (d) Raman spectra of PNA-15/5 hydrogels at 25 °C and 80 °C. (e) Variation of storage modulus (G') and loss modulus (G'') of PNA-15/5 hydrogel with temperature. (f) Variation of G′ and G″ of PNA-15/5 hydrogel with shear frequency tested at 25 °C.

hydrogel precursor for fiber spinning, because of its reversible transition between viscous spinning solution at elevated temperature and stable gel fibers at room temperature. These tests also indicated that the resulting PNA-15/5 hydrogel fibers don't dissolve in water and are stable in solid form when the temperature is lower than ~80 °C. Though this temperature limit may not be high, it is still suitable for E-textiles.

2.3. Mechanical, anti-evaporation, and self-healing properties

Uniaxial tensile tests were performed for hydrogel fibers at a rate of 50 mm min^{-1}. The tensile strength of PNA conductive hydrogel fiber (560 μm diameter) is 2.27 MPa, and the strain to failure can reach 900% (Fig. 3a). The PNA/PMA core-sheath fiber showed a slight decrease of the mechanical performances (2.25 MPa of tensile strength and 840% of strain to fracture), which was ascribed to the lower strength (1.79 MPa) and strain (583%) of the PMA coating (Fig. S7). It is worth emphasizing that the PMA coating was elastomeric, which ensured the stretchability of the core-sheath fiber. One single PNA/PMA fiber could easily lift a 50 g weight, due to its excellent strength and stretchability. Comparing to the counterpart PNA hydrogel film (1.23 MPa strength, Fig. S8), the strength of the PNA hydrogel fiber was improved, which was attributed to the increased alignment of polymer chains during the extruding process. This extrusion-induced strengthening effect was further confirmed by the diameter-dependence of the tensile performances (Fig. S9). The tensile strength increased with decreasing the diameter; while the failure strain showed a reverse trend. Reducing the spinning head diameter led to the increase in the shear stress and therefore the chain alignment. A similar trend was found in our previous work of polydimethylsiloxane luminescent fibers [37].

The water evaporation of hydrogel is still a major disadvantage for hydrogel electronics [13]. Here, the water evaporation of the PNA hydrogel fiber and PNA/PMA fiber was also tested at room temperature and relative humidity of ~40 RH%. The weight of both two fibers decreased dramatically in the first 12 days, but then maintained stable during the following period. After about 60 days, the weight retention ratio of the PNA/PMA and PNA hydrogel fiber is 67% and 42%, respectively (Fig. 3b), suggesting that the PMA coating is effective in confining the water in the core fiber. After 30 days, the tensile strength of PNA/PMA fiber decreased slightly to 1.77 MPa, and the strain to failure could still reach 680% (Fig. S10); while the bare PNA hydrogel fiber suffered from water-loss hardening, resulting in a sharp increase of tensile strength to 9.09 MPa and dramatic drop of the fracture strain to 142% (Fig. S11). PMA coating can also effectively prevent core fibers from absorbing water in highly humid environments. The mass change of PNA hydrogel fiber after immersing in DI water for 140 min was 617.9%, while the mass change of PNA/PMA under the same conditions was only 145.9% (Fig. S12). At 40 °C, the improved anti-evaporation property of the PNA/PMA fiber was also confirmed comparing with the PNA hydrogel fiber without the sheath coating (Fig. S13). Nevertheless, the water loss of both the two fibers was exacerbated at high temperature. Future works are still required for addressing this issue. Though the elastomer coating cannot completely block the permittivity of water molecules, it still greatly improved the resistance to water evaporation and absorption [26]. Another function of the PMA sheath is to insulate the inner hydrogel fibers, as shown in Fig. S14.

The PNA hydrogel fiber is self-healable, due to the existence of abundant dynamic hydrogen bonding. After being cut completely by a razor blade and healed at 45 °C for 10 min, the recovered tensile strength and fracture strain were 1.22 MPa and 504%, respectively, correspondent to a healing efficiency of 54% based on the strength (Fig. 3c). The healing efficiency could be improved to 85% after 10 min healing at 60 °C, and the fracture strain recovered to 690%. A Rhodamine B-dyed hydrogel fiber and an undyed hydrogel fiber were cut and aligned closely. After the self-healing treatment, the two hydrogel fibers were spliced into one fiber (the inset in Fig. 3d). One long PNA hydrogel fiber was cut into multiple short pieces, which were then spliced into a network (Fig. 3d). After keeping at 45 °C for 5 min, a healed net was formed which could stably carry a 20.4 g orange (Fig. 3d). Though the PMA coating is not intrinsically self-healing, the mechanical properties of the PNA/PMA fiber can also be recovered at 60 °C. The fracture strain of the self-healed PNA/PMA fiber was slightly lower than the self-healed PNA/PMA fiber (Fig. S15). This was attributed to the difficulty in exactly aligning the coatings and fiber cores of two cut fiber pieces.

Table S1 compares our hydrogel fibers with reported works [22,23,27,31,32,38–41]. Our hydrogel fibers simultaneously achieved facile synthesis, excellent electrical and mechanical properties, self-healing capability, and water-resistance stabilities.

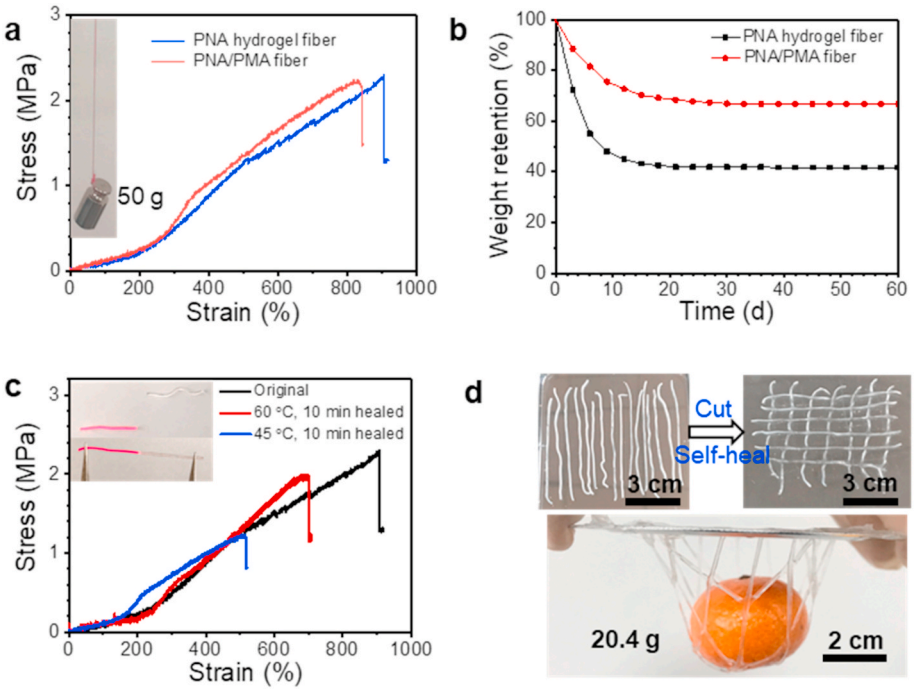

Fig. 3. Mechanical, anti-water-evaporation and self-healing properties. (a) Stress-strain curves of PNA and PNA/PMA hydrogel fibers at a tensile rate of 50 mm min^{-1}. The inset shows a PNA/PMA fiber lifting a 20 g weight. (b) Weight retention of PNA and PNA/PMA fibers along with time at room temperature and 40 RH%. (c) Stress-strain curves of the PNA hydrogel fiber before and after 10 min self-healing at 45 °C and 60 °C. The inset shows the photos of a cut PNA hydrogel fiber before and after the self-healing treatment. (d) Photos showing several PNA hydrogel fibers cut into short pieces and self-healed into a net, which can lift a 20.4 g orange. (For interpretation of the references to colour in this figure legend, the reader is referred to the Web version of this article.)

2.4. Strain sensing

The viability of applying the PNA/PMA fiber as a strain sensor has been demonstrated. The resistance (R) of the fiber increases as it is elongated, and the gauge factor (GF) of the fiber strain sensor is calculated as

$$GF = \frac{\delta(R - R_o)/R_o}{\delta\varepsilon} \quad (1)$$

where R_o is the original resistance before stretched, and ε is tensile strain. In the strain range 0–300%, the variation of $\Delta R/R_o$ ($\Delta R = R\text{-}R_o$) with ε can be fitted by quadratic polynomial curves (Fig. 4a), suggesting that the conductivity of the hydrogel fiber was not significantly varied and resistance variation was mainly due to the dimension change [14]. The gauge factor was 0.44–0.94 in the tested strain range, and almost increased linearly with the strain ε (the inset in Fig. 4a). The gauge factor is comparable with some reported hydrogel film-based strain sensors in the literature, as shown in Table S2 [39,42–46]. This fiber sensor also showed no noticeable hysteresis and relatively quick responses to tensile stimuli. As confirmed in Fig. 4b, the $\Delta R/R_o$ at each strain step (20% for each step except 10% for the last step) during the elongation process was about the same as that during the releasing process. Meantime, the response time for the elongation and releasing process of the fiber sensor was about 149 ms and 158 ms, respectively (Fig. S16). The low electrical hysteresis of the fiber sensor was due to its excellent resilience. As shown in Fig. S17, no noticeable hysteresis was observed from the strain-stress curves for the loading-unloading tests in the strain of 0–300%. The stability of the fiber sensor was confirmed by stretching-releasing cycling test conducted by a step motor. The fiber was 50% stretched and then released for 120 cycles, and $\Delta R/R_o$ showed stable and quick responses to the tensile stimuli throughout the cycling course (Fig. 4c and the inset). In addition, the electrical self-healing capability of the fiber sensor is also demonstrated. After being cut into three pieces and self-healed, the resistance of a PNA/PMA fiber only increased about 3% (Fig. S18). This slight increase in resistance is due to the misalignment of the cut fibers during the self-healing process. Excellent mechanical and electrical self-healing properties ensure the recovery of strain sensing capabilities.

For a demonstration of the strain sensing, the PNA/PMA fiber was connected to light a light-emitting diode (LED), whose brightness decreased when increasing the tensile strain from 0% to 300% (Fig. S19). It was also demonstrated that this fiber sensor can be used for monitoring the movement of human joints. One fiber was fixed on an index finger as a sensor to monitor the motion of the finger joint. The strain gauge could sense the flexion degree of the index finger through the electrical signal variation caused by bending the finger to different angles (Fig. 4d and e). Therefore, hand gestures could be possibly monitored and distinguished when fiber sensors were fixed on each of the five fingers. For example, the gesture of "ok", "victory" and "claw" showed distinctive electrical signals (Fig. 4f). The strain sensing capability of the PNA/PMA fiber suggests its potential in electronic textiles for sensors or human-machine interface applications.

2.5. Triboelectric energy harvesting

We further demonstrated the potentials of the PNA/PMA fibers in textile-based triboelectric nanogenerators (TENG) for generating electricity from mechanical motions. A TENG textile was simply woven from the PNA/PMA fibers, as schemed in Fig. 5a. The two photos in Fig. 5a show a piece of fabric woven solely from the PNA/PMA fibers with and without stretching deformation, respectively. This fabric was highly stretchable and soft due to the excellent stretchability of PNA/PMA fibers. The conductive core fibers functioned as the electrode; while the dielectric PMA sheath was the triboelectrification layer. The TENG textile worked in single-electrode mode, whose working mechanism is similar to the hydrogel-film-based TENGs [18]. As illustrated in Fig. 5b, when an alien material moves to contact the TENG fabric, equivalent amount of static charges with opposite polarities will be generated at the contacting interfaces [47]. Taking polytetrafluoroethylene (PTFE) as the counter material for example, the PMA will be positively charged. When the PTFE is separated from the fabric, the negative charges in the conductive hydrogel fibers will be induced to balance the local charge at the PNA/PMA interfaces, and electrons move from the ground to the PNA hydrogel/metal wire interfaces. Therefore, a current flows from the fiber electrode to the ground through the external circuit. The current will stop when the PTFE is far away and the static charges in PMA are all

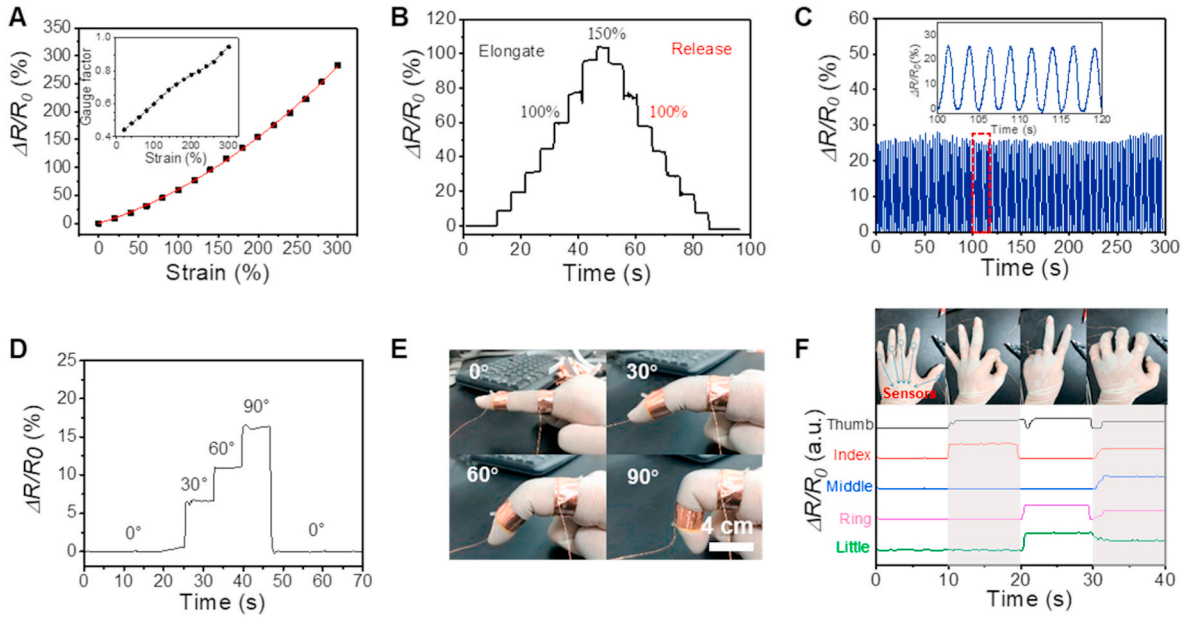

Fig. 4. Strain sensing performances of the PNA/PMA fibers. (a) Variation of $\Delta R/R_o$ of the fiber with the tensile strain. The inset is the calculated gauge factors. (b) Variation of $\Delta R/R_o$ with time during step-wise elongating and releasing process (20% strain for each step other than 10% for the top one). (c) Cycling stability of the fiber strain sensor. (d) Variation of $\Delta R/R_o$ with time of a fiber fixed on a finger bending for different angles, as shown by photos accordingly in (e). (f) Monitoring hand gestures with five fiber strain sensors fixed on five fingers.

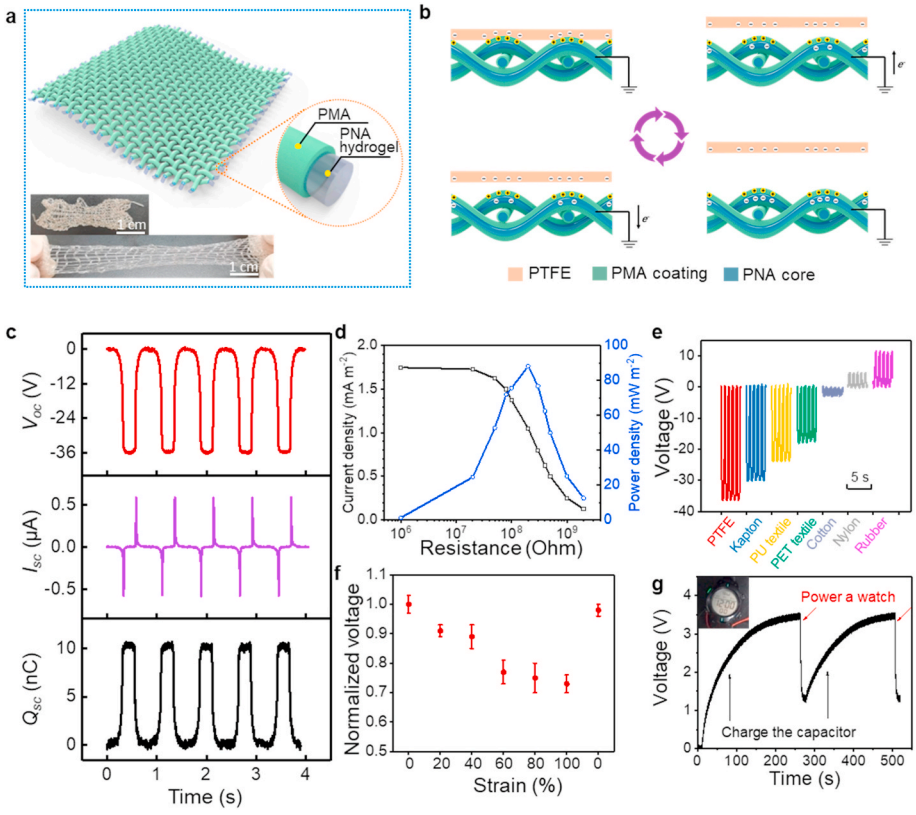

Fig. 5. Triboelectric nanogenerators textiles. (a) Schematic illustration a TENG textile woven from PNA/PMA core-sheath fibers. Two photos show a woven TENG textile without and with stretching deformation. (b) The mechanism of the TENG textile in contact-separation single-electrode mode. (c) The output V_{oc}, I_{sc}, and Q_{sc} of the TENG textile at a ~1.25 Hz relative motion to a PTFE film. (d) The variation of current density and peak power density with the external loading resistance. (e) V_{oc} of the TENG textile under contact-separation motion relative to different materials. PTFE, Kapton and nitrile rubber are films; PU textile (80% polyester +20% spandex), PET (polyester) textile, Cotton and Nylon are fabrics. (f) V_{oc} of the TENG textile when being stretched to different strains. (g) Voltage profile of a 6 μF capacitor when being charged by the TENG textile and used to power an electronic watch.

screened. Similarly, when PTFE approaches the TENG fabric again, charges will flow in the opposite directions, generating an opposite current in the circuit. Repeated contact-separation motions can produce a pulsed alternating current.

The output open-circuit voltage (V_{oc}) of the TENG textile reached −36 V when a ~1.25 Hz contact-separation motion relative to a PTFE film was applied by a linear motor (Fig. 5c). The pulsed AC short-circuit current (I_{sc}) reached an amplitude of ~0.7 μA, and the transferred charge quantity (Q_{sc}) was ~10 nC for each motion cycle. The TENG textile could be termed as a current source, whose output current did not decrease until the external resistance was larger than about 20 MOhm; meantime, the maximum peak power density of ~88 mW m^{-2} was obtained at a matched resistance of about 200 MOhm (Fig. 5d). The V_{oc} is positively proportional to the quantity of static charges generated at the contacting interfaces, which is higher if the triboelectric negativity difference of the two contacting materials is larger [48,49]. Therefore, it was concluded from Fig. 5e that the triboelectric negativity of the PMA coating is close to the cotton fabric; the nylon fabric and nitrile rubber (NBR) are more tribo-positive than PMA; while polyester fabric, spandex fabric and polyimide (Kapton) film are all more tribo-negative than PMA. To enlarge the output of the TENG textiles, fabrics fabricated from polyester, spandex and polyimide are better to be employed as the counter contacting materials.

The outputs of the TENG textile at stretched states were examined. The output V_{oc} decreased slightly when the TENG textile was stretched in the range of 0–100%. When the strain was released, the output voltage could be recovered (Fig. 5f). It is worth noting that the TENG still showed reliable stability after 1875 contact-separation cycles (Fig. S20). In order to demonstrate the potential of the TENG textile as a power source, the AC output was converted to DC power by a bridge rectifier and stored in a commercial capacitor (6 μF). The capacitor could be charged to 3.5 V in 260 s and then powered an electronic watch for 14 s (Fig. 5g). It should be noted that it is hard to recover the electricity generation of the TENG textile after damage, since the PMA layer is not intrinsically self-healable and the exact alignment of the thin fibers is difficult. The TENG textile woven from the PNA/PMA fibers was therefore demonstrated being applicable as soft, stretchable energy-harvesting devices for E-textiles.

3. Conclusion

In summary, a dry-wet spinning strategy was developed for continuous synthesis of PNA hydrogel fibers, which was realized due to the thermally reversible sol-gel transition achieved by optimizing the content ratio of AAm and NAGA. The physically cross-linked hydrogel fiber achieved excellent tensile performances, high conductivity and self-healing capability. With the elastomeric PMA coatings, the core-sheath fiber not only maintained the mechanical properties but also showed excellent resistance to water evaporation and absorbing. The strain sensing capability of the PNA/PMA fiber was demonstrated and applied for monitoring human body motions. Furthermore, a TENG textile woven from the PNA/PMA fibers was fabricated to convert mechanical motion energy into electricity. The potential of the stretchable TENG textile as a power source of wearable electronics was demonstrated. Therefore, our hydrogel fibers, with facile synthesis and excellent properties, can be highly promising for multifunctional smart textiles and wearable electronics.

4. Experimental section

4.1. Materials

Acrylamide (AAm, 98%, as a monomer), 2-potassium chloride (KCl, 99.5%), ethyl acetate (99%), methyl acrylate (MA, 99%), tetrahydrofuran (THF, 99%), and 2,2′-Azobis (isobutyronitrile) (AIBN, 99%) were purchased from Aladdin. Hydroxy-2-methyl-1-phenyl-1-propanone (photoinitiator 1173, 96%, as an initiator) was purchased from Tokyo Chemical Industry (TCI). N-acryloyl glycinamide (NAGA, 98%, as a

monomer) was purchased from Zhengzhou Alpha Chemical Industry. AIBN was recrystallized three times from ethanol.

4.2. Synthesis of PNA hydrogel fibers and PNA/PMA fibers

The optimal PNA hydrogel preparation procedure is as follows: 150 mg NAGA powder, 50 mg AAm and 50 mg LiCl were dissolved in 750 ml deionized water and shaken for 30 min to obtain a homogeneous solution. Then 1 wt% of the photoinitiator IRGACURE 1173 was added to the clear solution and shaken for 30 min to form a homogeneous mixture. The solution was placed in a transparent spinning storage tank and polymerized in an ultraviolet light source box (ZF-20D) for 40 min under UV light at 365 nm to form a hydrogel. Use a heating mantle to heat the storage tank to 90 °C to soften the PNA hydrogel. The softened hydrogel was extruded from the spinning head into ethyl acetate as a coagulation bath to obtain stable PNA hydrogel fibers. The formed PNA fibers were further immersed in a 5 wt% PMA ethyl acetate solution for 30 s, and then taken out to evaporate the ethyl acetate solvent to obtain PNA/PMA fibers.

4.3. Characterization of PNA hydrogel fibers and PNA/PMA fibers

The tensile test of the PNA hydrogel fiber and PNA/PMA fiber was implemented with an INSTRON tensile tester (INSTRON 5944, USA) in extension mode (tensile rate of 50 mm min^{-1}). Rheology tests were performed with the Anton-Paar rheometer (MCR 302, Austria). All samples were made into films with a diameter of 25 mm and a thickness of 1 mm. Dynamic mechanical analysis (DMA) was performed for the samples to test the temperature dependence of the storage and loss modulus of the PNA hydrogel (temperature range 25–90 °C). The storage modulus and loss modulus were measured by a small amplitude shear oscillation in the linear region at a constant shear rate (1–100 rad s^{-1}).

CRediT authorship contribution statement

Luyizheng Shuai: Formal analysis, fabricated the fibers, textiles and related characterizations, wrote the paper, to which all authors provided feedback. **Zihao Guo:** Formal analysis, wrote the paper, to which all authors provided feedback. **Panpan Zhang:** aided in the dynamic mechanical measurements. **Junmin Wan:** Supervision. **Xiong Pu:** Supervision, wrote the paper, to which all authors provided feedback. **Zhong Lin Wang:** Supervision.

Declaration of competing interest

The authors declare that they have no known competing financial interests or personal relationships that could have appeared to influence the work reported in this paper.

Acknowledgements

The authors thank for the support from the Youth Innovation Promotion Association of CAS, the Zhejiang Top Priority Discipline of Textile Science and Engineering, Natural Science Foundation of Zhejiang Province (No. LY13B030009), Science Foundation of Zhejiang Sci-Tech University (ZSTU) (No. 1101820-Y).

Appendix A. Supplementary data

Supplementary data to this article can be found online at https://doi.org/10.1016/j.nanoen.2020.105389.

References

[1] J. Shi, S. Liu, L. Zhang, B. Yang, L. Shu, Y. Yang, M. Ren, Y. Wang, J. Chen, W. Chen, Y. Chai, X. Tao, Smart textile-integrated microelectronic systems for wearable applications, Adv. Mater. 32 (2020), 1901958.
[2] W. Weng, P. Chen, S. He, X. Sun, H. Peng, Smart electronic textiles, Angew. Chem. Int. Ed. 55 (2016) 6140–6169.
[3] A.K. Yetisen, H. Qu, A. Manbachi, H. Butt, M.R. Dokmeci, J.P. Hinestroza, M. Skorobogatiy, A. Khademhosseini, S.H. Yun, Nanotechnology in textiles, ACS Nano 10 (2016) 3042–3068.
[4] G. Chen, Y. Li, M. Bick, J. Chen, Smart textiles for electricity generation, Chem. Rev. 120 (2020) 3668–3720.
[5] M. Liu, Z. Cong, X. Pu, W. Guo, T. Liu, M. Li, Y. Zhang, W. Hu, Z.L. Wang, High-energy asymmetric supercapacitor yarns for self-charging power textiles, Adv. Funct. Mater. 29 (2019), 1806298.
[6] M. Zhang, K.R. Atkinson, R.H. Baughman, Multifunctional carbon nanotube yarns by downsizing an ancient technology, Science 306 (2004) 1358–1361.
[7] Z. Xu, C. Gao, Graphene chiral liquid crystals and macroscopic assembled fibres, Nat. Commun. 2 (2011) 571.
[8] N. Behabtu, C.C. Young, D.E. Tsentalovich, O. Kleinerman, X. Wang, A.W.K. Ma, E. A. Bengio, R.F. ter Waarbeek, J.J. de Jong, R.E. Hoogerwerf, S.B. Fairchild, J. B. Ferguson, B. Maruyama, J. Kono, Y. Talmon, Y. Cohen, M.J. Otto, M. Pasquali, Strong, light, multifunctional fibers of carbon nanotubes with ultrahigh conductivity, Science 339 (2013) 182–186.
[9] P. Miaudet, S. Badaire, M. Maugey, A. Derré, V. Pichot, P. Launois, P. Poulin, C. Zakri, Hot-drawing of single and multiwall carbon nanotube fibers for high toughness and alignment, Nano Lett. 5 (2005) 2212–2215.
[10] S.-W. Kim, S.-N. Kwon, S.-I. Na, Stretchable and electrically conductive polyurethane- silver/graphene composite fibers prepared by wet-spinning process, Compos. B Eng. 167 (2019) 573–581.
[11] S. Seyedin, J.M. Razal, P.C. Innis, A. Jeiranikhameneh, S. Beirne, G.G. Wallace, Knitted strain sensor textiles of highly conductive all-polymeric fibers, ACS Appl. Mater. Interfaces 7 (2015) 21150–21158.
[12] S. Zhu, J.-H. So, R. Mays, S. Desai, W.R. Barnes, B. Pourdeyhimi, M.D. Dickey, Ultrastretchable fibers with metallic conductivity using a liquid metal alloy core, Adv. Funct. Mater. 23 (2013) 2308–2314.
[13] C. Yang, Z. Suo, Hydrogel ionotronics, Nat. Rev. Mater. 3 (2018) 125–142.
[14] C. Keplinger, J.-Y. Sun, C.C. Foo, P. Rothemund, G.M. Whitesides, Z. Suo, Stretchable, transparent, ionic conductors, Science 341 (2013) 984–987.
[15] Z. Wang, Y. Cong, J. Fu, Stretchable and tough conductive hydrogels for flexible pressure and strain sensors, J. Mater. Chem. B 8 (2020) 3437–3459.
[16] B. Chen, Y. Bai, F. Xiang, J.-Y. Sun, Y. Mei Chen, H. Wang, J. Zhou, Z. Suo, Stretchable and transparent hydrogels as soft conductors for dielectric elastomer actuators, J. Polym. Sci. B Polym. Phys. 52 (2014) 1055–1060.
[17] C.H. Yang, B. Chen, J. Zhou, Y.M. Chen, Z. Suo, Electroluminescence of giant stretchability, Adv. Mater. 28 (2016) 4480–4484 (n/a-n/a).
[18] X. Pu, M. Liu, X. Chen, J. Sun, C. Du, Y. Zhang, J. Zhai, W. Hu, Z.L. Wang, Ultrastretchable, transparent triboelectric nanogenerator as electronic skin for biomechanical energy harvesting and tactile sensing, Sci. Adv. 3 (2017), e1700015.
[19] K. Parida, V. Kumar, W. Jiangxin, V. Bhavanasi, R. Bendi, P.S. Lee, Highly transparent, stretchable, and self-healing ionic-skin triboelectric nanogenerators for energy harvesting and touch applications, Adv. Mater. 29 (2017), 1702181.
[20] N.A. Choudhury, S. Sampath, A.K. Shukla, Hydrogel-polymer electrolytes for electrochemical capacitors: an overview, Energy Environ. Sci. 2 (2009) 55–67.
[21] Y. Wu, D.U. Shah, C. Liu, Z. Yu, J. Liu, X. Ren, M.J. Rowland, C. Abell, M. H. Ramage, O.A. Scherman, Bioinspired supramolecular fibers drawn from a multiphase self-assembled hydrogel, Proc. Natl. Acad. Sci. Unit. States Am. 114 (2017) 8163–8168.
[22] Y. Dou, Z.-P. Wang, W. He, T. Jia, Z. Liu, P. Sun, K. Wen, E. Gao, X. Zhou, X. Hu, J. Li, S. Fang, D. Qian, Z. Liu, Artificial spider silk from ion-doped and twisted core-sheath hydrogel fibres, Nat. Commun. 10 (2019) 5293.
[23] X. Zhao, F. Chen, Y. Li, H. Lu, N. Zhang, M. Ma, Bioinspired ultra-stretchable and anti-freezing conductive hydrogel fibers with ordered and reversible polymer chain alignment, Nat. Commun. 9 (2018) 3579.
[24] M.S. Austero, A.E. Donius, U.G.K. Wegst, C.L. Schauer, New crosslinkers for electrospun chitosan fibre mats. I. Chemical analysis, J. R. Soc. Interface 9 (2012) 2551–2562.
[25] C.H. Yang, B. Chen, J.J. Lu, J.H. Yang, J. Zhou, Y.M. Chen, Z. Suo, Ionic cable, Extreme Mech. Lett. 3 (2015) 59–65.
[26] P. Le Floch, X. Yao, Q. Liu, Z. Wang, G. Nian, Y. Sun, L. Jia, Z. Suo, Wearable and washable conductors for active textiles, ACS Appl. Mater. Interfaces 9 (2017) 25542–25552.
[27] J. Guo, X. Liu, N. Jiang, A.K. Yetisen, H. Yuk, C. Yang, A. Khademhosseini, X. Zhao, S.H. Yun, Highly stretchable, strain sensing hydrogel optical fibers, Adv. Mater. 28 (2016) 10244–10249.
[28] C.M. Hwang, A. Khademhosseini, Y. Park, K. Sun, S.-H. Lee, Microfluidic chip-based fabrication of PLGA microfiber scaffolds for tissue engineering, Langmuir 24 (2008) 6845–6851.
[29] M.A. Daniele, S.H. North, J. Naciri, P.B. Howell, S.H. Foulger, F.S. Ligler, A. A. Adams, Rapid and continuous hydrodynamically controlled fabrication of biohybrid microfibers, Adv. Funct. Mater. 23 (2013) 698–704.
[30] C.K. Lee, S.R. Shin, S.H. Lee, J.-H. Jeon, I. So, T.M. Kang, S.I. Kim, J.Y. Mun, S.-S. Han, G.M. Spinks, G.G. Wallace, S.J. Kim, DNA hydrogel fiber with self-entanglement prepared by using an ionic liquid, Angew. Chem. Int. Ed. 47 (2008) 2470–2474.

[31] J. Fei, Z. Zhang, L. Zhong, L. Gu, PVA/PAA thermo-induced hydrogel fiber: preparation and pH-sensitive behavior in electrolyte solution, J. Appl. Polym. Sci. 85 (2002) 2423–2430.
[32] K. Hou, H. Wang, Y. Lin, S. Chen, S. Yang, Y. Cheng, B.S. Hsiao, M. Zhu, Large scale production of continuous hydrogel fibers with anisotropic swelling behavior by dynamic-crosslinking-spinning, Macromol. Rapid Commun. 37 (2016) 1795–1801.
[33] X. Dai, Y. Zhang, L. Gao, T. Bai, W. Wang, Y. Cui, W. Liu, A mechanically strong, highly stable, thermoplastic, and self-healable supramolecular polymer hydrogel, Adv. Mater. 27 (2015) 3566–3571.
[34] Z. Xu, W. Liu, Poly(N-acryloyl glycinamide): a fascinating polymer that exhibits a range of properties from UCST to high-strength hydrogels, Chem. Commun. 54 (2018) 10540–10553.
[35] Z. Ahmed, E.A. Gooding, K.V. Pimenov, L. Wang, S.A. Asher, UV resonance Raman determination of molecular mechanism of poly(N-isopropylacrylamide) volume phase transition, J. Phys. Chem. B 113 (2009) 4248–4256.
[36] L.B. Sagle, Y. Zhang, V.A. Litosh, X. Chen, Y. Cho, P.S. Cremer, Investigating the hydrogen-bonding model of urea denaturation, J. Am. Chem. Soc. 131 (2009) 9304–9310.
[37] W. Ding, J. Sun, G. Chen, L. Zhou, J. Wang, X. Gu, J. Wan, X. Pu, B. Tang, Z. L. Wang, Stretchable multi-luminescent fibers with AIEgens, J. Mater. Chem. C 7 (2019) 10769–10776.
[38] S. Sun, A.F.T. Mak, The dynamical response of a hydrogel fiber to electrochemical stimulation, J. Polym. Sci. B Polym. Phys. 39 (2001) 236–246.
[39] J. Song, S. Chen, L. Sun, Y. Guo, L. Zhang, S. Wang, H. Xuan, Q. Guan, Z. You, Mechanically and electronically robust transparent organohydrogel fibers, Adv. Mater. 32 (2020), 1906994.
[40] C. Chen, J. Tang, Y. Gu, L. Liu, X. Liu, L. Deng, C. Martins, B. Sarmento, W. Cui, L. Chen, Bioinspired hydrogel electrospun fibers for spinal cord regeneration, Adv. Funct. Mater. 29 (2019), 1806899.
[41] T. Yin, L. Wu, T. Wu, G. Mao, G. Nian, Z. Chen, X. Hu, P. Wang, Y. Xiang, H. Yu, S. Qu, W. Yang, Ultrastretchable and conductive core/sheath hydrogel fibers with multifunctionality, J. Polym. Sci. B Polym. Phys. 57 (2019) 272–280.
[42] Y.-J. Liu, W.-T. Cao, M.-G. Ma, P. Wan, Ultrasensitive wearable soft strain sensors of conductive, self-healing, and elastic hydrogels with synergistic “soft and hard” hybrid networks, ACS Appl. Mater. Interfaces 9 (2017) 25559–25570.
[43] Z. Wang, H. Zhou, J. Lai, B. Yan, H. Liu, X. Jin, A. Ma, G. Zhang, W. Zhao, W. Chen, Extremely stretchable and electrically conductive hydrogels with dually synergistic networks for wearable strain sensors, J. Mater. Chem. C 6 (2018) 9200–9207.
[44] J.-Y. Sun, C. Keplinger, G.M. Whitesides, Z. Suo, Ionic skin, Adv. Mater. 26 (2014) 7608–7614.
[45] R. Tong, G. Chen, D. Pan, J. Tian, H. Qi, R.a. Li, F. Lu, M. He, Ultrastretchable and antifreezing double-cross-linked cellulose ionic hydrogels with high strain sensitivity under a broad range of temperature, ACS Sustain. Chem. Eng. 7 (2019) 14256–14265.
[46] S. Liu, L. Li, Ultrastretchable and self-healing double-network hydrogel for 3D printing and strain sensor, ACS Appl. Mater. Interfaces 9 (2017) 26429–26437.
[47] Z.L. Wang, A.C. Wang, On the origin of contact-electrification, Mater. Today 30 (2019) 34–51.
[48] S. Niu, Z.L. Wang, Theoretical systems of triboelectric nanogenerators, Nano Energy 14 (2015) 161–192.
[49] Z.L. Wang, On Maxwell’s displacement current for energy and sensors: the origin of nanogenerators, Mater. Today 20 (2017) 74–82.